Triplet Formation on a Monomeric Chlorophyll in the Photosystem II Reaction Center As Studied by Time-Resolved Infrared Spectroscopy

Takumi Noguchi,*,‡ Tatsuya Tomo,§ and Chihiro Kato||

Biophysical Chemistry Laboratory, RIKEN, Wako, Saitama 351-0198, Japan, Laboratory for Photo-Biology, RIKEN Photodynamics Research Center, Aoba, Sendai, Miyagi 980-0845, Japan, and Basic Technology Division, Kanagawa Industrial Technology Research Institute, Ebina, Kanagawa 243-0435, Japan

Received August 21, 2000; Revised Manuscript Received November 28, 2000

ABSTRACT: The process of formation of the triplet state of chlorophyll in the photosystem II (PS II) reaction center complex was studied by means of time-resolved infrared (IR) spectroscopy. Using a dispersive-type IR spectrometer with a time resolution of ∼55 ns, transient spectra in the C═O stretching region (1760−1600 cm^{-1}) were measured at 77 K. The data were analyzed by singular-value decomposition and subsequent least-squares fitting. Two distinct spectral components having different kinetic behaviors were resolved. One had spectral features characterized by negative peaks at 1740 and 1680 cm^{-1} and an overall positive background and was assigned to the $P_{680}^+Phe^-/P_{680}Phe$ radical pair by static FTIR measurements of the P_{680}^+/P_{680} and Phe^-/Phe differences. The other had prominent negative and positive peaks at 1668 and 1628 cm^{-1}, respectively, which were previously assigned to the keto C═O change upon triplet formation of the monomeric chlorophyll denoted as Chl_T [Noguchi, T., Tomo, T., and Inoue, Y. (1998) *Biochemistry 37,* 13614−13625]. The former component of $P_{680}^+Phe^-/P_{680}Phe$ exhibited a multiphasic decay with time constants of 77 ns (75%), 640 ns (18%), 8.3 μs (4%), and 0.3 ms (3%), while the latter component of $^3Chl_T/Chl_T$ was formed with a single-exponential rise with a time constant of 57 ns and had a lifetime of 1.5 ms. From the observations that only the two spectral components were resolved without any other triplet intermediates and the time constant of $^3Chl_T$ formation roughly agreed with or seemed even faster than that of the major phase of the $P_{680}^+Phe^-$ decay, two alternative mechanisms of triplet formation are proposed. (i) $^3Chl_T$ is directly formed from $P_{680}^+Phe^-$ by charge recombination at Chl_T, and (ii) $^3P_{680}$ is formed, and then the triplet is transferred to Chl_T with a time constant of much less than 50 ns. The location of Chl_T in the D1 subunit as the monomer chlorophyll corresponding to the accessory bacteriochlorophyll in the L subunit of purple bacteria is favored to explain the former mechanism as well as the triplet properties reported in the literature. The physiological role of the triplet formation on Chl_T is also discussed.

In photosystem II (PS II)[1] of green plants, algae, and cyanobacteria, light energy is used to drive charge separation between the primary donor chlorophyll (P_{680})[2] and the pheophytin electron acceptor (Phe). The electron is subsequently transferred from Phe^- to the primary (Q_A) and then the secondary (Q_B) quinone acceptors. On the electron donor side, the hole moves from P_{680}^+ to the tyrosine Y_Z and then to the Mn cluster, where water is oxidized and molecular oxygen is evolved [reviews by Diner and Babcock (*1*) and Satoh (*2*)]. It has been suggested that the PS II RC evolved from quinone-type bacterial RC, which is typically seen in purple photosynthetic bacteria (*3*). In fact, the amino acid sequences of the D1 and D2 subunits of the PS II RC closely resemble those of the L and M subunits of the bacterial RC, and the electron-transfer components on the acceptor side agree between both the RCs, although the components on the donor side are rather different and the oxygen-evolving devices are absent in the bacterial RC. The similarity of the two RCs was also recently demonstrated by the three-dimensional electron microscopic structure of PS II obtained with 8 Å resolution (*4*), in which the locations of the transmembrane helices of the D1 and D2 subunits are in good agreement with those of the bacterial L and M subunits.

PS II RC proteins can be purified as the D1−D2−cyt b_{559} complex (*5*). This RC complex binds six chlorophylls, two

* To whom correspondence should be addressed. Phone: +81-48-462-1111, ext 5461. Fax: +81-48-462-4660. E-mail: tnoguchi@postman.riken.go.jp.

‡ RIKEN.

§ RIKEN Photodynamics Research Center.

|| Kanagawa Industrial Technology Research Institute.

[1] Abbreviations: B_L and B_M, accessory bacteriochlorophylls in the L and M subunits, respectively, in bacterial reaction centers; Chl_T, monomeric chlorophyll that mainly carries the triplet state in photosystem II; ENDOR, electron nuclear double resonance; EPR, electron paramagnetic resonance; FTIR, Fourier transform infrared; fwhm, full width at half-maximum; IR, infrared; IRF, instrumental response function; P, primary electron donor of bacterial reaction centers; P_{680}, primary electron donor of photosystem II; Phe, pheophytin electron acceptor of photosystem II; PS II, photosystem II; Q_A, primary quinone electron acceptor of photosystem II; Q_B, secondary quinone electron acceptor of photosystem II; RC, reaction center; SVD, singular-value decomposition.

[2] In this paper, we use the term "P_{680}" for the chlorophylls that possess a delocalized positive charge after the initial charge separation in PS II (*25*). These chlorophylls probably correspond to the special pair in bacterial RCs. The lowest excited singlet state that initiates charge separation could be on a different chlorophyll or on an excitonically coupled multimer of chlorophylls and pheophytins (*62*).

10.1021/bi0019848 CCC: $20.00
Published on Web 01/27/2001

pheophytins, and two β-carotenes, and is depleted of the Mn cluster and the Q_A and Q_B quinone acceptors (reviewed in ref *2*). The PS II RC complex can perform primary charge separation, and the radical pair $P_{680}^+Phe^-$ is formed upon excitation. Because of the absence of Q_A, however, further electron transfer is blocked, and the $P_{680}^+Phe^-$ recombines with a $\tau_{1/2}$ of ~55 ns at 5 K, forming a triplet state of chlorophyll (*6*). This chlorophyll triplet decays with a $\tau_{1/2}$ of ~0.9 ms at 5−120 K (*6*). The similar triplet formation of chlorophyll by radical pair recombination has also been observed in PS II membrane preparations when Q_A is doubly reduced or depleted (*7, 8*). This triplet formation is thought to be involved in the photoinhibition process, in which harmful singlet oxygen is produced by triplet transfer followed by specific degradation of the D1 polypeptide (*8*).

Until recently, the triplet state produced in the PS II RC has been thought to be located on P_{680}. This idea was based on (i) the observation that the peak position of the Q_y bleach upon triplet formation was found at about 680 nm (*9*−*14*), which was similar to the peak position upon P_{680}^+ formation (*15*−*18*), and (ii) the analogy to the bacterial RC [when triplet transfer to carotenoid is absent (*19*)] and PS I, in which the triplet state resides on the primary donor (*20*, *21*). However, this idea has been controversial, because the EPR spectra of triplet chlorophyll in PS II exhibited a monomeric nature and the ring orientation that is about parallel to the membrane plane (*22*), in contrast to the dimeric, perpendicular structure of bacterial P (*23*). In fact, to reconcile these inconsistent properties, various models of the P_{680} structure have been proposed such as a monomeric chlorophyll or a T-shape asymmetric dimer (reviewed in ref *1*). The recent electron microscopic structure, however, showed the presence of two chlorophylls at the positions analogous to those of the bacterial special pair with a slightly larger center−center distance (*4*). Also, ENDOR (*24*) and FTIR (*25*) studies suggested that the positive charge on P_{680} is delocalized over chlorophyll molecules, being inconsistent with the monomeric P_{680} model.

Identification of each chlorophyll molecule in the PS II RC complex using a Q_y absorption band is much more difficult than the case of bacterial RC because the Q_y bands of all the six chlorophylls and two pheophytins overlap in the narrow wavelength region of 670−685 nm. In contrast, IR absorption of the keto C═O stretching vibration of chlorophyll or pheophytin shows a band in the relatively wide range of 1710−1620 cm^{-1}, and its position varies depending on the hydrogen-bonding strength and electrostatic environment (*26*−*29*). Thus, IR spectroscopy is a useful tool for distinguishing among individual chlorophyll and pheophytin molecules having different binding sites in proteins. The previous light-induced FTIR difference spectrum of the PS II RC complex upon triplet formation exhibited a prominent negative peak at 1669 cm^{-1}, which was first assigned to the keto C═O of P_{680} in accordance with the conventional idea of triplet formation on P_{680} (*30*). The P_{680}^+/P_{680} FTIR spectrum recorded recently (*25, 31*), however, did not exhibit a negative band at this position and instead exhibited bands at 1704 and 1679 cm^{-1} that are possible candidates of the keto C═O of P_{680} (*25, 31*). From this observation, it was concluded that the triplet state mainly resides on a monomeric chlorophyll different from P_{680} (*25, 31*), and this chlorophyll was denoted as Chl_T (*25*). Indeed, this idea explains all the controversial observations about P_{680} and the triplet state mentioned above.

The above view that the triplet state in the PS II RC resides on the monomer chlorophyll Chl_T raises new questions about the mechanism of triplet formation. Is the triplet state formed first on P_{680} and then transferred to Chl_T, in a manner similar to the triplet transfer from P to carotenoid in bacterial RC? Are there other mechanisms for forming $^3Chl_T$, like direct formation upon charge recombination or triplet transfer using unknown intermediates? To answer these questions, in this study, we have investigated the process of triplet formation in the PS II RC complex by means of time-resolved IR spectroscopy. We used a time-resolved instrument with a dispersive-type IR spectrometer having a time resolution of ~55 ns. The data were analyzed by singular-value decomposition (SVD) in combination with least-squares fitting. With the results that we obtained, we discuss the mechanism of triplet formation, the location of Chl_T, and the physiological role of triplet formation on Chl_T.

MATERIALS AND METHODS

The PS II RC complex (D1−D2−cyt b_{559}) was isolated from spinach as described in ref *32*, followed by replacement of the original detergent (Triton X-100) with 0.2% *n*-dodecyl β-D-maltoside. The RC sample was dissolved in 10 mM Hepes/NaOH buffer (pH 7.5) including 0.1% dodecyl maltoside, and stored at −80 °C until it was used. For IR measurements, the RC sample (1.4 mg of chlorophyll/mL; 3−6 μL) was cast on a CaF_2 plate (13 mm ϕ), lightly dried under a N_2 gas flow, and then covered with another CaF_2 plate. The sample temperature was controlled in a liquid N_2 cryostat (Oxford, model DN1704) using a temperature controller (Oxford, model ITC-5). The absorbance of the amide I peak at 1656 cm^{-1} was ~0.5 for time-resolved IR measurements and ~1.0 for static FTIR difference measurements.

Transient IR spectra were measured using a nanosecond time-resolved system with a dispersive-type IR spectrometer (*33*). The sample was excited by the second harmonic (532 nm) of a diode laser-pumped Q-switched Nd:YAG laser (Continuum HPO-1000) [pulse width, ~10 ns (fwhm); repetition, 300 Hz; power, 1 mJ/pulse; beam diameter at the sample, 2−4 mm]. Monitoring light from a $MoSi_2$ IR source (JASCO) (~1700 K) was dispersed with an IR grating monochromator (modified model IR-700 from JASCO) after passing through the sample placed between two ellipsoidal mirrors, and focused onto a photovoltaic MCT detector (Kolmar Technologies, model KV104-1-A50-3). Scattered light of the pump laser was removed with a KRS-5 window placed in front of the entrance slit of the IR monochromator. The intensity change of the IR light induced by photoreaction was extracted by an AC-coupled preamplifier (modified model KA020-A1A from Kolmer; 2.5 Hz ~ 20 MHz bandwidth). The signal was then amplified again with a second amplifier (NF Electronic Instruments, model 5305; 10 MHz bandwidth) and recorded on a 1 GHz digital oscilloscope (LeCroy model LC534A). The bandwidth of the second amplifier was limited to 1 MHz for the 100 ns/point and 5 μs/point measurements to reduce higher-frequency noise. The measurements were performed in the three temporal regions: from −5 to 45 μs with 10 ns/point,

from −10 to 90 μs with 100 ns/point, and from −0.5 to 4.5 ms with 5 μs/point. The transient signal was recorded and averaged 4096 times at each fixed wavenumber. The monochromator was controlled by a personal computer and scanned from 1760 to 1600 cm^{-1} every 4 cm^{-1}. The spectral resolution was 16 cm^{-1}. The scan process was repeated 16 times, twice, and once for the 10 ns/point, 100 ns/point, and 5 μs/point measurements, respectively. The instrumental response function (IRF) of this apparatus was obtained by detecting the scattered light of a laser pulse with the MCT detector. The time giving the maximal intensity of IRF was regarded as time zero. The two-dimensional data with temporal and spectral axes of the 10 ns/point measurement were further analyzed by singular-value decomposition (SVD) and least-squares fitting using the IGOR Pro program (Wavemetrics Inc.). Before the SVD analysis, the data were smoothed along the time axis using a binomial function with five points in IGOR Pro.

Static light-induced FTIR difference spectra were recorded on a Bruker IFS-66/S FTIR spectrophotometer equipped with an MCT detector (EG&G JUDSON, model J15D16-M200B-S01M-60). P_{680}^{+}/P_{680}, Phe^{-}/Phe, and triplet/singlet difference spectra of the PS II RC complex were measured following the methods of Noguchi et al. (*25*), Nabedryk et al. (*34*), and Noguchi et al. (*30*), respectively. The P_{680}^{+}/P_{680} difference spectra were measured at 150 K in the presence of potassium ferricyanide as an electron acceptor after photobleaching of redox-active β-carotene by preillumination at 250 K (*25*). The Phe^{-}/Phe spectra were measured at 240 K in the presence of sodium dithionite as an electron donor (*34*). For both P_{680}^{+}/P_{680} and Phe^{-}/Phe pairs, difference spectra were obtained by subtraction between the two single-beam spectra recorded before (100 s) and under (100 s) continuous-light illumination. The triplet/singlet spectra were measured at 77 K by the dark-and-light cycle (1 s−1 s) repeated 500 times, instead of the original method of longer accumulation (10 s) and subsequent subtraction of thermal bands (*30*). As light sources, a halogen lamp equipped with heat-cut and red (>600 nm) filters (∼20 mW/cm^2 at the sample) was used for the P_{680}^{+}/P_{680} and Phe^{-}/Phe measurements, and a 600 W tungsten lamp through a cold filter (Nihon Shinku Kogaku type B) (∼500 mW/cm^2) was used for the triplet/singlet measurement. Spectra were measured with resolutions of both 4 and 16 cm^{-1}.

RESULTS

Time-resolved IR spectra in the C═O region (1760−1600 cm^{-1}) as absorbance changes upon laser pulse excitation measured at 77 K are shown in Figure 1. The spectra represent the time regions of −30 to 70 ns (a), 70−170 ns (b), 1−2 μs (c), 80−90 μs (d), 0.5−1.0 ms (e), and 1.0−1.5 ms (f). The features of the spectrum in the earliest time region (−30 to 70 ns) are distinct from those of the other spectra. The most prominent characteristic of this spectrum is high positive background in the overall region. On this background, several negative peaks at 1740, 1680, 1652, and 1624 cm^{-1} and positive peaks at 1708, 1660, and 1636 cm^{-1} were observed. This first spectrum then converts to the spectrum with a simpler shape of negative and positive peaks at 1668 and 1628 cm^{-1}, respectively, which decays in milliseconds. The latter peak pair is typical of the keto C═O change upon formation of the triplet state of chlorophyll in the PS II RC complex, which has been detected in static light-induced FTIR difference spectra (*30*).

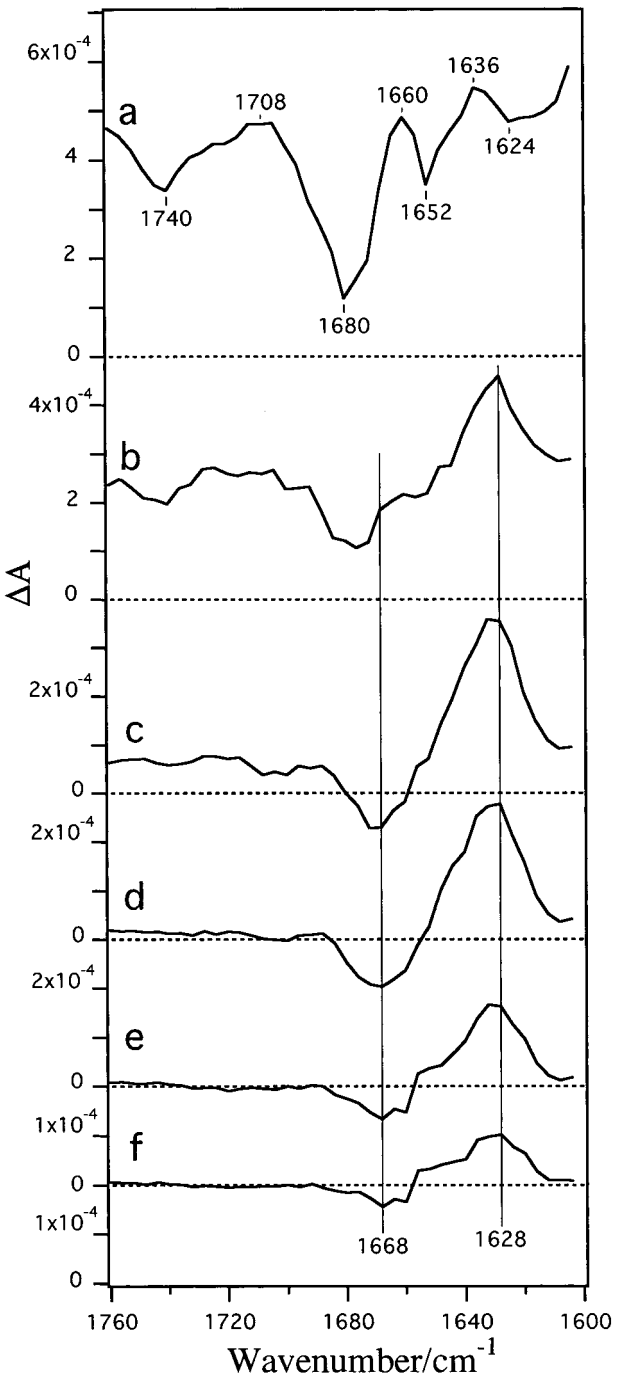

FIGURE 1: Time-resolved IR spectra of the PS II RC complex upon excitation with a laser pulse (532 nm, ∼10 ns). The spectra represent the changes in the time regions of −30 to 70 ns (a), 70−170 ns (b), 1−2 μs (c), 80−90 μs (d), 0.5−1.0 ms (e), and 1.0−1.5 ms (f). A zero line ($\Delta A = 0$) is shown as a dashed line in each panel. Spectra a and b were obtained as the average of 10 spectra in the 10 ns/point measurement, spectra c and d as the average of 10 and 100 spectra, respectively, in the 100 ns/point measurement, and spectra e and f as the average of 100 spectra in the 5 μs/point measurement. The sample temperature was 77 K. The spectral resolution was 16 cm^{-1}.

In Figure 2 are shown the time courses of the intensity changes at 1628, 1668, and 1760 cm^{-1}. At 1760 cm^{-1}, no signal due to triplet formation was observed (*30*), and hence, only the contribution of the positive background due to the early component is expected. Three time domains up to 600

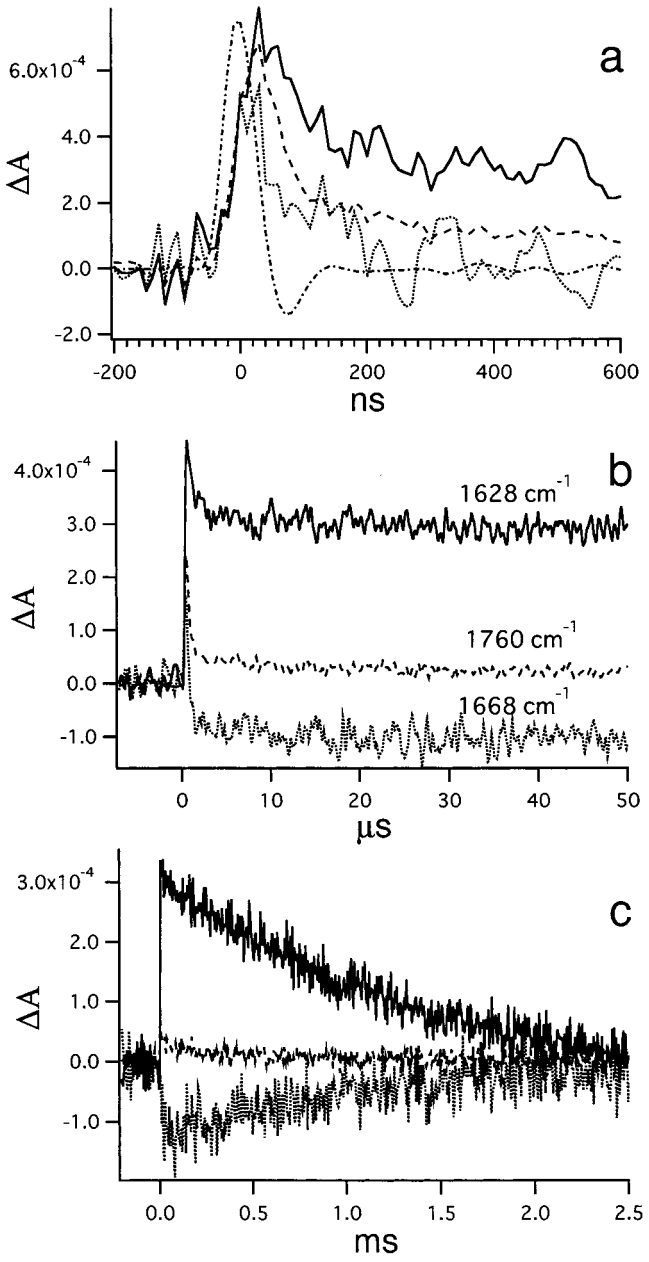

FIGURE 2: Time course of IR absorbance change measured at 1628 (—), 1668 (•••), and 1760 (– – –) cm^{-1} in the nanosecond (a), microsecond (b), and millisecond (c) time domains. The instrumental response function (IRF) is shown in panel a (—•—). The IRF exhibits a full width at half-maximum of 55 ns, which corresponds to the time resolution of the instrument. The data were measured with 10 ns/point (a), 100 ns/point (b), and 5 μs/point (c). The sample temperature was 77 K.

ns (a), 50 μs (b), and 2.5 ms (c) are presented. The instrumental response function (IRF) is also shown in panel a (—•—). The IRF exhibits a fwhm of 55 ns, which corresponds to the time resolution of the instrument. It is noted that the IRF has a overshooting negative peak after the main positive peak. This feature is due to the transient response character of the first amplifier.

The IR intensity at 1760 cm^{-1} rises immediately after the pulse excitation, and exhibits a multiphasic decay. Most of the population decays with a time constant similar to the instrumental time resolution [Figure 2a (– – –)]. The minor decay phases were resolved in panels b and c of Figure 2 (– – –), and their time constants were estimated to be 8 μs and 0.3 ms. The time courses of the intensity changes at 1628 and 1668 cm^{-1} also follow that of the 1760 cm^{-1} intensity in the early time region (<200 ns) (Figure 2a). This is mainly due to the overlap of the positive background at these wavenumbers as seen in Figure 1a. The 1628 and 1668 cm^{-1} intensities then reach stable positive and negative values, respectively, in the microsecond region (Figure 2b). Both intensities decay with a time constant of 1.5 ms (Figure 2c).

The time-dependent behaviors of all the spectral components in the early nanosecond time domain cannot be resolved in the raw data given above because of the severe spectral overlap. To overcome this difficulty, SVD analysis (*35*–*37*) was applied to the data measured between −5 and 45 μs with 10 ns/point (see the Supporting Information for the details of the SVD analysis). Because the spectra were recorded from 1760 to 1600 cm^{-1} every 4 cm^{-1}, the complete data set is expressed with a matrix (**A**) of 5000 × 41 data points along the time and wavenumber axes. The SVD calculation of matrix **A** gave only two significant singular values, indicating that two components are involved in this time-resolved data and other components are regarded as noise. The kinetic profiles (t_1 and t_2) of the two spectral components obtained by the SVD calculation are expressed as linear combinations of the kinetic profiles (t_a and t_b) of the physically meaningful spectral components. It is expected that t_a and t_b have the decaying and rising curves expressed by the IRF convolution of multiexponentials. By the least-squares fit of t_1 and t_2, such exponential functions that give the best fit were obtained as

$$f_a = 0.75\exp(-t/77\text{ ns}) + 0.18\exp(-t/640\text{ ns}) + 0.04\exp(-t/8.3\,\mu\text{s}) + 0.03$$

$$f_b = 1 - \exp(-t/57\text{ ns})$$

Figure 3 shows the resultant fitting functions [f_a and f_b convoluted with the IRF (—)], together with the experimental kinetic curves [t_a and t_b (•••)]. The last constant of f_a is considered to correspond to the 0.3 ms decay phase, which was observed in the intensity change at 1760 cm^{-1} (Figure 2c). Also, the 8.3 μs phase agrees with the minor decay phase of 8 μs in Figure 2b. From these results, it is concluded that the decaying component (Figure 3a,c) has four phases with time constants of 77 ns (75%), 640 ns (18%), 8.3 μs (4%), and 0.3 ms (3%). The calculation also showed that the rising component (Figure 3b,d) has a single phase with a time constant of 57 ns.

The spectral components corresponding to the decaying and rising kinetic curves are shown in panels a and b of Figure 4, respectively. The former spectrum is similar to the raw spectrum of the −30 to 70 ns region (Figure 1a) immediately after the pulse excitation. The latter spectrum exhibits negative and positive peaks at 1668 and 1628 cm^{-1}, respectively, that are characteristic of the spectra by triplet formation observed in the late time region (Figure 1c–f). Note that the minor bands at ~1720/1700 cm^{-1} in Figure 4b are probably due to an artifact from degraded centers, because this signal becomes larger after longer data accumulation. This signal was also observed in the original time-resolved spectra (for example, Figure 1c). Since this signal has a shape of the upshifted keto C═O band, which is typical

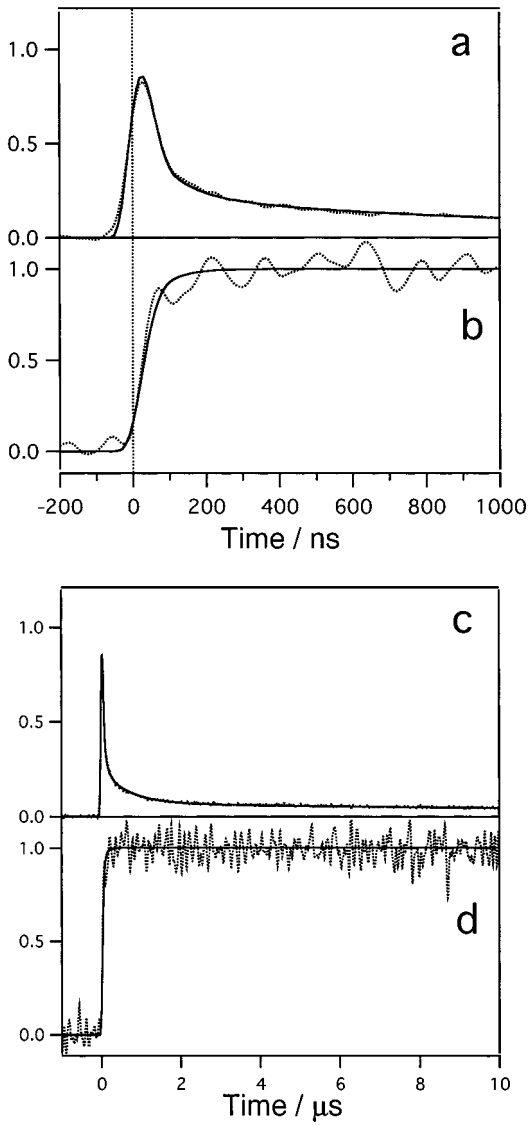

FIGURE 3: Kinetic profiles of the two components as the result of SVD analysis and subsequent least-squares fitting using exponentials convoluted with the IRF. The time regions of −200 to 1000 ns and −1 to 10 μs are shown in panels a and b and in panels c and d, respectively. Solid curves are the fitting functions of exponentials convoluted with the IRF, and dotted curves are the corresponding experimental data. The decaying component (a and c) was fit by three exponentials with time constants of 77 ns (75%), 640 ns (18%), and 8.3 μs (4%) and a constant (3%). The rising component (b and d) was fit with a single-exponential function with a time constant of 57 ns.

of the cation formation of chlorophyll (*38*), it might be due to the cation formation of some chlorophylls in impaired proteins, but the precise origin of this signal is unknown at present.

The above transient IR spectra were all measured with a relatively low spectral resolution of 16 cm^{-1} to obtain a signal/noise ratio sufficient for the data analysis. Hence, the spectra cannot be compared directly with the authentic spectra that have been obtained by static FTIR measurements typically using 4 cm^{-1} resolution. To identify the spectral species observed in the time-resolved measurements, we have measured static light-induced FTIR difference spectra of P_{680}^+/P_{680}, Phe^-/Phe, and triplet/singlet with resolutions of both 4 and 16 cm^{-1}. Figure 5 shows the C═O stretching region (1760−1600 cm^{-1}) of the spectra that were obtained.

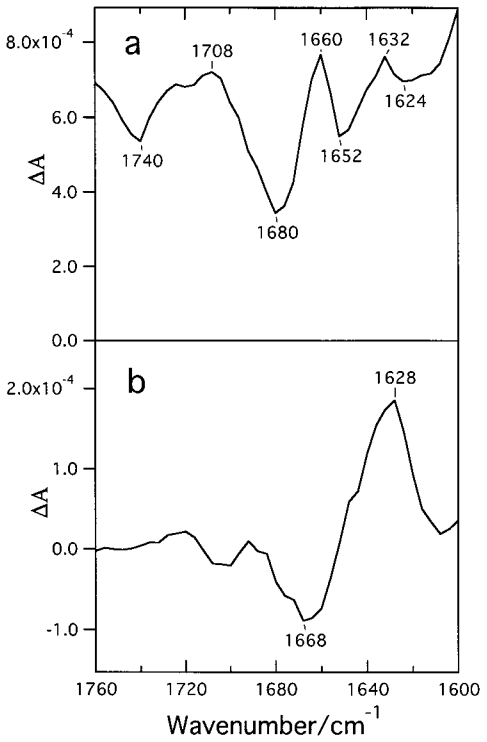

FIGURE 4: Two spectral components as the result of SVD analysis and subsequent least-squares fitting of the kinetic profiles (Figure 3). Spectra a and b correspond to the kinetic profiles in panels a and c and in panels b and d of Figure 3, respectively.

The P_{680}^+/P_{680} difference spectrum with 4 cm^{-1} resolution [Figure 5a (···)] is characterized by a negative peak at 1704 cm^{-1} and positive peaks at 1729 and 1711 cm^{-1}, which have been tentatively assigned to the C═O stretching bands of P_{680} and P_{680}^+, respectively, and a signal at 1664/1655 cm^{-1}, which may arise from the backbone amide C═O stretching (*25*). By lowering the resolution to 16 cm^{-1} [Figure 1a (—)], the former peaks of keto C═O are altered into a broad differential signal at 1720/1693 cm^{-1} (two peaks at 1729 and 1711 cm^{-1} are not resolved at this resolution), while the latter signal is left at 1666/1651 cm^{-1}. Other minor features at 4 cm^{-1} resolution (e.g., the peak at 1679 cm^{-1}) disappeared at 16 cm^{-1} resolution. As previously reported by Noguchi et al. (*25*), one of the characteristics of the P_{680}^+/P_{680} spectrum is a positive broad feature centered at 1940 cm^{-1}, which arises from the electronic transition of the charge-delocalized chlorophyll dimer. The contribution of this broad electronic absorption is clearly seen as a positive background in the overall C═O region of the spectrum with 16 cm^{-1} resolution [Figure 5a (—)].

The Phe^-/Phe spectrum with 4 cm^{-1} resolution [Figure 5b (···)] was basically identical to the spectrum obtained by Nabedryk et al. (*34*). The prominent negative and positive bands at 1678 and 1587 cm^{-1}, respectively (the latter band is not shown in Figure 5), were assigned to the keto C═O bands of Phe and Phe^- (*34*). In the region of carbomethoxy C═O and carboxylic acid (1700−1750 cm^{-1}), negative peaks at 1740 and 1722 cm^{-1} and positive peaks at 1730 and 1701 cm^{-1} were observed. With 16 cm^{-1} resolution [Figure 5b (—)], only negative bands at 1743 and 1678 cm^{-1} and a positive band at 1701 cm^{-1} are left as prominent features.

The FTIR spectrum upon radical pair formation, P_{680}^+-Phe^-/P_{680}Phe, with 16 cm^{-1} resolution was produced by

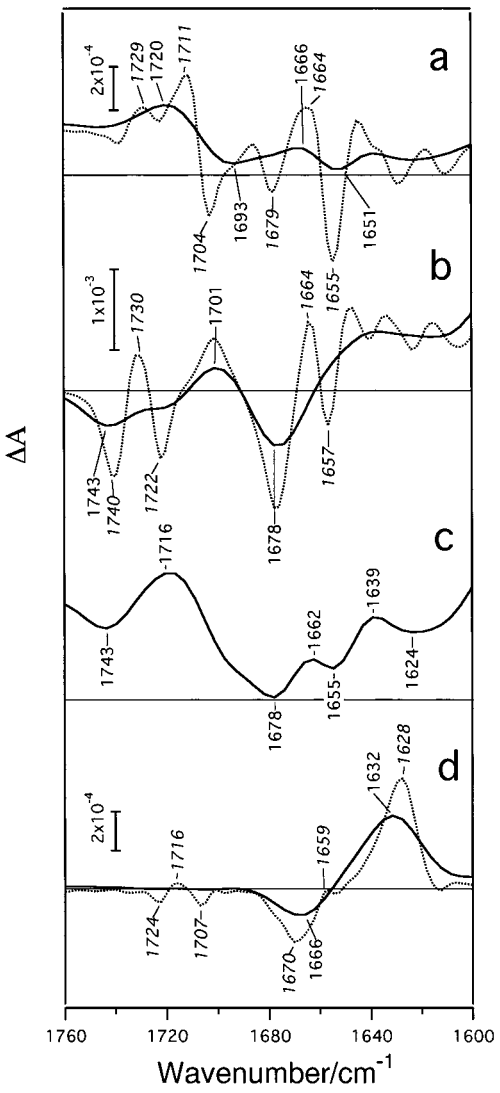

FIGURE 5: Static light-induced FTIR difference spectra in the C═O stretching region of P_{680}^+/P_{680} (a), Phe^-/Phe (b), $P_{680}^+Phe^-/P_{680}$Phe (c), and triplet/singlet (d) measured with the PS II RC complex. Spectra were obtained with a resolution of 4 (···) and 16 (—) cm^{-1}. Spectrum a was measured at 150 K in the presence of potassium ferricyanide, and spectrum b was measured at 240 K in the presence of sodium dithionite. Spectrum c was calculated by addition of spectra a and b after normalization of intensities on the basis of the keto C═O bands (see the text). Spectrum d was measured at 77 K.

adding the P_{680}^+/P_{680} [Figure 5a (—)] and Phe^-/Phe [Figure 5b (—)] spectra after normalization at the 1720/1693 (P_{680}^+/P_{680}) and 1587/1678 (Phe^-/Phe) cm^{-1} bands, both of which have been ascribed to the keto C═O vibrations. The resultant spectrum (Figure 5c) was characterized by the peaks at 1743(−), 1716(+), 1678(−), 1662(+), 1655(−), 1639(+), and 1624(−) cm^{-1} (+ and − in parentheses mean positive and negative peaks, respectively). These peaks correspond well to those at 1740(−), 1708(+), 1680(−), 1660(+), 1652(−), 1632−1636(+), and 1624(−) cm^{-1} of the transient spectrum of the −30 to 70 ns region (Figure 1a) and of the spectrum of the decaying component obtained by SVD analysis (Figure 4a). The positive background of these spectra was also reproduced in the composed $P_{680}^+Phe^-/P_{680}$Phe spectrum (Figure 5c). Thus, the initially produced and rapidly decaying component in the time-resolved spectra (Figures 1a and 4a) is reasonably attributed to the $P_{680}^+Phe^-$ radical pair. The prominent negative peaks at 1740 and 1680 cm^{-1} in Figures 1a and 4a are conceived to originate from the Phe change, and the negative peak at 1652 cm^{-1} and the overall positive background from the P_{680} change. The negative C═O band at 1693 cm^{-1} in the P_{680}^+/P_{680} spectrum with 16 cm^{-1} resolution [Figure 5a (—)] seems to be canceled out by the positive feature of the Phe^-/Phe spectrum at 1701 cm^{-1} [Figure 5b (—)], showing no prominent peak at this position in the $P_{680}^+Phe^-/P_{680}$Phe spectrum (Figures 1a, 4a, and 5c).

The triplet/singlet spectrum measured at 77 K with 4 cm^{-1} resolution [Figure 5d (···)] was characterized by large negative and positive bands at 1670 and 1628 cm^{-1} (*30*) arising from the keto C═O of Chl_T and $^3Chl_T$, respectively (*25*). The minor band pair at 1707 and 1659 cm^{-1} has been attributed to another chlorophyll in triplet equilibrium with $^3Chl_T$, which has been suggested to be a chlorophyll(s) in P_{680} (*25*). A small differential signal at 1724/1716 cm^{-1} may arise from the carbomethoxy C═O of Chl_T. At 16 cm^{-1} resolution, the small features at 1724, 1716, 1707, and 1659 cm^{-1} all disappeared, and only the major peaks of Chl_T were left at slightly shifted positions of 1666 and 1632 cm^{-1} [Figure 5d (—)]. These two bands correspond to the 1668 and 1628 cm^{-1} bands in the time-resolved spectra in the microsecond to millisecond region (Figure 1c−f) and in the spectrum of the rising component obtained by SVD analysis (Figure 4b). The absence of the small peaks at 1724, 1716, and 1707 cm^{-1} in the spectrum with 16 cm^{-1} resolution is consistent with a rather flat feature in this region of the time-resolved spectra in the late time region (e.g., Figure 1e,f).

In the time-resolved spectrum of the $P_{680}^+Phe^-/P_{680}$Phe pair (Figures 1a and 4a), no peak was observed at 1668−1670 cm^{-1}, where Chl_T has a keto C═O band (Figures 1c−f, 4b, and 5d). This observation confirms the previous conclusion that Chl_T, where the triplet state is mainly localized, is a chlorophyll molecule different from P_{680} that possesses a positive charge after initial charge separation (*25*, *31*).

DISCUSSION

Mechanism of Triplet Formation in the PS II RC. Time-resolved IR measurements with a time resolution of ∼55 ns (fwhm of the IRF) at 77 K in combination with SVD and fitting analyses revealed two spectral components having different temporal behaviors (Figures 1−4). The first one is due to the formation of the $P_{680}^+Phe^-$ radical pair, which is characterized by a high positive background of P_{680}^+ and a prominent negative band at 1680 cm^{-1} arising from the keto C═O of Phe. This radical pair component mostly (75%) decayed with a time constant of 77 ns ($\tau_{1/2}$ = 54 ns) (Figure 3a). This value is consistent with the reported decay rate of the $P_{680}^+Phe^-$ pair obtained by time-resolved absorption measurements in the visible region: $\tau_{1/2}$ = 55 ns at 5 K and $\tau_{1/2}$ = 40 ns at 135 K (*6*). The $P_{680}^+Phe^-$ decay exhibited minor phases with time constants of 640 ns (18%), 8.3 μs (4%), and 0.3 ms (3%) (Figures 2 and 3). This multiphasic decay might be due to the heterogeneity of the RC sample or the partially impaired center.

The second spectral component is ascribed to the triplet formation on Chl_T, which was characterized by negative and

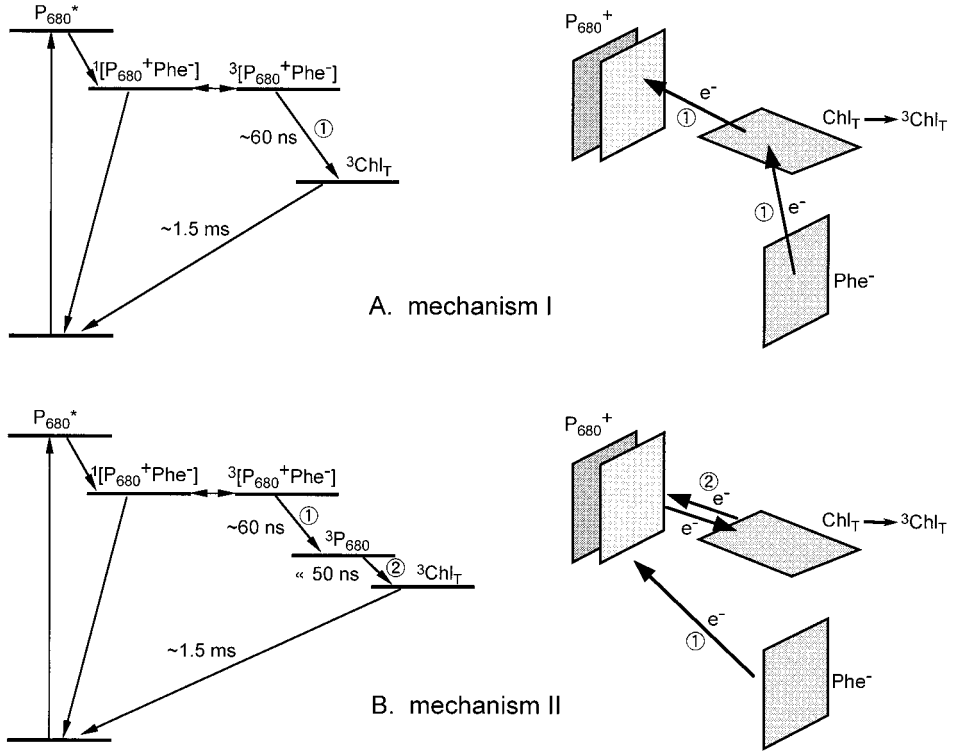

FIGURE 6: Proposed mechanisms of triplet formation in the PS II RC. In mechanism I (A), $^3Chl_T$ is directly formed from the $P_{680}^+Phe^-$ radical pair by charge recombination at Chl_T. This is a one-step process in which electrons move from Phe^- to Chl_T and from Chl_T to P_{680}^+ in a concerted way. In mechanism II (B), $^3P_{680}$ is first formed by charge recombination and then the triplet state is transferred to Chl_T rapidly ($\ll$50 ns). This is a two-step process in which an electron moves from Phe^- to P_{680}^+ and then Dexter-type electron exchange occurs between $^3P_{680}$ and Chl_T.

positive bands at 1668 and 1628 cm^{-1} arising from the keto C═O vibrations of Chl_T and $^3Chl_T$, respectively. The rise of the $^3Chl_T/Chl_T$ signal was fit by a single-exponential function with a time constant of 57 ns (Figure 3b). The $^3Chl_T$ decayed with a time constant of 1.5 ms ($\tau_{1/2}$ = 1.0 ms), which is consistent with the previous $\tau_{1/2}$ value of 0.9 ms at 5−120 K (*6*). The fact that the $^3Chl_T$ rise could be fit with only a single-exponential function means that the minor slow phases of the $P_{680}^+Phe^-$ decay do not form a triplet state and thus probably directly relax to the ground state. The small discrepancy between the time constant of the major $P_{680}^+Phe^-$ decay (77 ns) and that of the $^3Chl_T$ rise (57 ns) may be attributed to the limitation of time resolution (∼55 ns). Alternatively, this is possibly because the 77 ns decay actually includes another minor phase that does not convert into the triplet state and has a time constant slightly greater than 57 ns.

From the results that only the two spectral components, $P_{680}^+Phe^-/P_{680}Phe$ and $^3Chl_T/Chl_T$, were resolved and the rates of the $P_{680}^+Phe^-$ decay and the $^3Chl_T$ formation had similar values or the latter seemed rather faster, the following two mechanisms of triplet formation can be considered (Figure 6). (i) Charge recombination of $^3[P_{680}^+Phe^-]$ directly produces $^3Chl_T$ (mechanism I), and (ii) $^3P_{680}$ is once formed, and then the triplet state is transferred to Chl_T with a rate much faster than 50 ns (mechanism II). If Chl_T is located between P_{680} and Phe as will be discussed below, then mechanism I of direct $^3Chl_T$ formation has an advantage over mechanism II. In this case, the separated charges on P_{680}^+ and Phe^- recombine at Chl_T; in other words, the electrons move from Phe^- to Chl_T and from Chl_T to P_{680} in a concerted way (Figure 6A). This mechanism requires the shortest distance of electron movement to produce $^3Chl_T$, and thus, the potential barrier is expected to be small.

On the other hand, mechanism II is analogous to the triplet formation in bacterial RCs. In RCs of purple bacteria, the triplet state is once formed on P by charge recombination and then is transferred to the carotenoid in the M subunit through the accessory bacteriochlorophyll B_M (*39*−*42*). Since the energy level of ^3B_M is higher than that of ^3P, ^3B_M actually works as a potential barrier in the triplet transfer to the carotenoid (*39*−*42*). It is known that in the PS II RC, the triplet state produced by charge recombination is not transferred to the β-carotene bound to the RC proteins (*6*). Thus, in mechanism II, the triplet state once formed on P_{680} is transferred to another accessory chlorophyll Chl_T, which has a lower triplet level than P_{680}. Mechanism II is a two-step process in contrast to the one-step process of mechanism I. The electron is transferred from Phe^- to P_{680}^+ first, and then the triplet transfer occurs by the Dexter-type electron exchange mechanism (*43*) (Figure 6B). In the RC of wild type *Rhodobacter sphaeroides*, the rate of triplet transfer from P to the carotenoid has been estimated to be faster than 50 ns (*40*, *44*) even with a potential barrier of ∼200 cm^{-1} by ^3B_M (*39*−*41*). Hence, it is likely that in the PS II RC where no specific energy barrier is expected between $^3P_{680}$ and $^3Chl_T$, the rate of triplet transfer from P_{680} to Chl_T is much faster than 50 ns, and thus $^3P_{680}$ cannot be detected as an intermediate.

Although the triplet state is mostly localized on Chl_T at cryogenic temperatures, the triplet is shared with another chlorophyll(s) as a thermal equilibrium at higher temperatures (*30*, *45*, *46*). We previously suggested that this triplet equilibrium is between Chl_T and P_{680} from the frequency of

the minor keto C═O peak in the triplet/singlet FTIR difference spectrum (1707 cm^{-1}) similar to that of the major C═O peak in the P_{680}^+/P_{680} difference spectrum (1704 cm^{-1}) (*25*). The energy gap was estimated to be 8−13 meV by FTIR (*30*) and EPR (*45*, *46*) studies. By extrapolation of the temperature dependence plot in the FTIR study (*30*), it is estimated that more than 70% of the triplet state is located on Chl_T even at 20 °C. In contrast to this triplet location in PS II, in bacterial RCs from carotenoid-less strains, the triplet state resides on P (*20*, *21*, *40*, *44*). This inconsistency between PS II and the bacterial RC may simply be attributed to the triplet energy levels of (bacterio)chlorophyll cofactors. In bacterial RCs, the triplet levels of monomeric bacteriochlorophylls are higher than that of P (*40*−*42*), whereas the energy level of $^3Chl_T$ is lower than that of $^3P_{680}$ in PS II.

Where Is Chl_T Located? The PS II RC has six chlorophyll molecules. Two of them are the chlorophyll dimer P_{680}, which possesses a delocalized cation charge after the initial charge separation (*24*, *25*). Chl_Z is the monomer chlorophyll that is oxidized when the Mn cluster is depleted and is thought to be attached to D1 His118 or D2 His118 (*3*, *47*−*50*). Chl_D is the symmetric counterpart of Chl_Z (*47*). The remaining two chlorophylls are probably the analogues of the accessory bacteriochlorophylls, B_L and B_M, in the bacterial RC. We propose that Chl_T, which carries the triplet state, is the monomeric chlorophyll in the D1 subunit corresponding to B_L for the following reasons. (i) The present time-resolved IR data indicated the two possible mechanisms of $^3Chl_T$ formation, i.e., direct $^3Chl_T$ formation from the radical pair (mechanism I) and rapid triplet transfer from $^3P_{680}$ to Chl_T (mechanism II). Both mechanisms require the Chl_T location in the close vicinity of P_{680} or the $P_{680}^+Phe^-$ radical pair. In particular, mechanism I (Figure 6A) is best explained when the Chl_T is located between P_{680} and Phe (see above). Chl_Z and Chl_D are thought to be located rather apart from P_{680} (*49*, *50*). (ii) The keto C═O frequency of Chl_T (1668−1670 cm^{-1}) (Figures 1, 4b, and 5d) is at odds with those of P_{680} (1704 and/or 1679 cm^{-1}) (Figure 5a) (*25*, *31*) and of Chl_Z (1684 cm^{-1}) (*51*), and thus, these chlorophylls are excluded from the candidates. (iii) The macrocycle of Chl_T is oriented about parallel to the membrane plane (*22*), and this orientation, together with the ring rotation angle (*14*), is almost the same as that of bacterial B_L or B_M. The parallel orientation is consistent with neither Chl_Z nor Chl_D, whose ring is expected to be oriented about perpendicular to the membrane (*3*, *49*, *50*). (iv) The lifetime of $^3Chl_T$ is significantly shortened by the presence of Q_A^- (see below) (*52*), and hence, Chl_T should be located close to Q_A. Thus, the accessory chlorophyll on the D1 side is preferred to that on the D2 side. (v) The D1 protein is selectively degraded by singlet oxygen produced via the triplet chlorophyll (*8*), suggesting that Chl_T is on the D1 side.

If Chl_T is a chlorophyll analogue of the accessory bacteriochlorophyll in the bacterial RC, what is the reason that $^3Chl_T$ is not quenched by β-carotene? The triplet energy level of β-carotene (*53*) is estimated to be lower than that of chlorophyll *a* (*41*), and indeed, triplet transfer from light-harvesting chlorophyll *a* to carotenoid has been observed in LHC II, CP43, CP47, and the peridinin−chlorophyll *a*−protein complex (*54*−*56*). Two β-carotene molecules are present in the PS II RC complex, whereas in the bacterial RC, only one carotenoid is bound to the M subunit. The close contact of the donor and acceptor molecules is necessary for triplet transfer by the Dexter mechanism (*43*). At least one of the two β-carotenes is electronically coupled to P_{680} probably through an accessory chlorophyll, because one β-carotene is selectively oxidized by P_{680} in the PS II RC complex at cryogenic temperatures (*25*). One possible reason for the absence of triplet transfer to β-carotene is that the two carotenoid molecules have highly asymmetric binding positions in the PS II RC; the redox-active β-carotene is in contact with the accessory chlorophyll analogous to the carotenoid in the bacterial RC, whereas the other β-carotene, which may be present on the same side as Chl_T, is located apart from chlorophylls. In fact, the two β-carotene molecules have rather different absorption maxima with the 0−0 peaks at 507 and 489 nm, and also, the measurements of linear dichroism showed that these carotenoids have significantly different orientations (*57*−*59*). The redox-active β-carotene is more red-shifted (0−0 peak at 507 nm), being consistent with the presence of strong electronic coupling with chlorophylls. If it is assumed that Chl_T is located on the D1 side, the carotenoids with 489 and 507 nm 0−0 peaks are located on the D1 and D2 sides, respectively. This location of carotenoids is consistent with the view by Tomo et al. (*59*) proposed from fluorescence measurements.

Physiological Role of Triplet Formation on Chl_T. Van Mieghem et al. (*52*) reported that the triplet state of chlorophyll produced from the radical pair in PS II decays much faster (2−20 μs) in the presence of Q_A^- than in the presence of Q_AH_2 (1−3 ms), and this is the reason the triplet state is not detected with Q_A^- in conventional EPR measurements. The shorter triplet lifetime in the presence of Q_A^- has been known for ^3P in the bacterial RC as well, but the effect is much smaller; the decay of ^3P in the RC of *Rb. sphaeroides* R-26 is only 7.5 times faster with Q_A^- than it is with Q_AH_2 at 293 K, and the Q_A^- effect was not seen at <160 K (*60*). Thus, it is assumed that the location of the triplet state on Chl_T rather than P_{680} is related to the larger effect (∼100 times larger than that of the bacterial RC) of Q_A^- in PS II. Deligiannakis and Rutherford (*61*) discussed the reason for the short lifetime of the triplet state in the presence of Q_A^- and favored the idea of the electron transfer quenching mechanism (*52*); that is, the Phe triplet is formed possibly as a virtual intermediate, and an electron transfer occurs from Q_A^- to ^3Phe to produce Phe^-, which then reduces Q_A. As pointed out by Deligiannakis and Rutherford (*61*), this mechanism explains the difference in the extent of the Q_A^- effect between PS II and the bacterial RC, if Chl_T is the counterpart of B_L that is adjacent to Phe.

In the process of photoinhibition, strong illumination first evacuates Q_B and forms Q_A^-, and then Q_A is doubly reduced and stabilized as a form of Q_AH_2, which finally leaves its binding site (*8*). In the early stage of photoinhibition, i.e., when Q_A is only singly reduced, the PS II function can fully recover in the dark by Q_A^- decay in a relatively short period of time (30 s half-time) (*8*). In this stage, the triplet state produced by charge recombination is quenched rapidly by Q_A^- (*52*) to prevent the formation of harmful singlet oxygen. In contrast, once Q_AH_2 is formed, it does not decay for a long period of 0.5−2 h, and when it leaves the Q_A pocket, the PS II function does not recover any more (*8*). In these stages of photoinhibition, the triplet state of Chl_T has a long

lifetime of milliseconds, and as a result, singlet oxygen is produced and the D1 protein selectively degraded (*8*).

Summarizing the above considerations, we infer the physiological roles of the triplet formation on Chl_T as follows: (i) protection of the PS II proteins against the damage by singlet oxygen using the Q_A^--induced triplet quenching in the early stage of photoinhibition and (ii) promoting degradation of the D1 protein by producing singlet oxygen in the late stage of photoinhibition. The PS II RC with doubly reduced Q_A or in the absence of Q_A takes a long time to recover or does not recover at all, and thus needs to be decomposed and replaced as soon as possible. The long lifetime of $^3Chl_T$ (~1.5 ms) relative to that of bacterial ^3P [$\tau_{1/2} < 150$ μs at 77 K in the carotenoid-less strains of *Rb. sphaeroides* (*40*, *44*)] and the absence of triplet transfer to carotenoid are "advantageous" to this degradation function. In addition, the proposed Chl_T location on the D1 side may be relevent to the selective degradation of the D1 protein.

SUPPORTING INFORMATION AVAILABLE

Details of the SVD analysis. This material is available free of charge via the Internet at http://pubs.acs.org.

REFERENCES

1. Diner, B. A., and Babcock, G. T. (1996) in *Oxygenic Photosynthesis: The Light Reactions* (Ort, D. R., and Yocum, C. F., Eds.) pp 213−247, Kluwer, Dordrecht, The Netherlands.
2. Satoh, K. (1996) in *Oxygenic Photosynthesis: The Light Reactions* (Ort, D. R., and Yocum, C. F., Eds.) pp 193−211, Kluwer, Dordrecht, The Netherlands.
3. Michel, H., and Deisenhofer, J. (1988) *Biochemistry 27*, 1−7.
4. Rhee, K.-H., Morris, E. P., Barber, J., and Kühlbrandt, W. (1998) *Nature 396*, 283−286.
5. Nanba, O., and Satoh, K. (1987) *Proc. Natl. Acad. Sci. U.S.A. 84*, 109−112.
6. Takahashi, Y., Hansson, Ö., Mathis, P., and Satoh, K. (1987) *Biochim. Biophys. Acta 893*, 49−59.
7. Van Mieghem, F. J. E., Nitschke, W., Mathis, P., and Rutherford, A. W. (1989) *Biochim. Biophys. Acta 977*, 207−214.
8. Vass, I., Styring, S., Hundal, T., Koivuniemi, A., Aro, E.-M., and Andersson, B. (1992) *Proc. Natl. Acad. Sci. U.S.A. 89*, 1408−1412.
9. Den Blanken, H. J., Hoff, A. J., Jongenelis, A. P. J. M., and Diner, B. A. (1983) *FEBS Lett. 157*, 21−27.
10. Van der Vos, R., van Leeuwen, P. J., Braun, P., and Hoff, A. J. (1992) *Biochim. Biophys. Acta 1140*, 184−198.
11. Carbonera, D., Giacometti, G., and Agostini, G. (1994) *FEBS Lett. 343*, 200−204.
12. Hillmann, B., Brettel, K., van Mieghem, F., Kamlowski, A., Rutherford, A. W., and Schlodder, E. (1995) *Biochemistry 34*, 4814−4827.
13. Eijckelhoff, C., Vacha, F., van Grondelle, R., Dekker, J. P., and Barber, J. (1997) *Biochim. Biophys. Acta 1318*, 266−274.
14. Kwa, S. L. S., Eijckelhoff, C., van Grondelle, R., and Dekker, J. P. (1994) *J. Phys. Chem. 98*, 7702−7711.
15. Telfer, A., and Barber, J. (1989) *FEBS Lett. 246*, 223−228.
16. Van Kan, P. J. M., Otte, S. C. M., Kleinherenbrink, F. A. M., Nieveen, M. C., Aartsma, T. J., and van Gorkom, H. J. (1990) *Biochim. Biophys. Acta 1020*, 146−152.
17. Groot, M.-L., van Mourik, F., Eijckelhoff, C., van Stokkum, I. H. M., Dekker, J. P., and van Grondelle, R. (1997) *Proc. Natl. Acad. Sci. U.S.A. 94*, 4389−4394.
18. Vacha, F., Joseph, D. M., Durrant, J. R., Telfer, A., Klug, D. R., Porter, G., and Barber, J. (1995) *Proc. Natl. Acad. Sci. U.S.A. 92*, 2929−2933.
19. Cogdell, R. J., and Frank, H. A. (1987) *Biochim. Biophys. Acta 895*, 63−79.
20. Budil, D. E., and Thurnauer, M. C. (1991) *Biochim. Biophys. Acta 1057*, 1−41.
21. Angerhofer, A. (1991) in *Chlorophylls* (Scheer, H., Ed.) pp 945−991, CRC Press, Boca Raton, FL.
22. Van Mieghem, F. J. E., Satoh, K., and Rutherford, A. W. (1991) *Biochim. Biophys. Acta 1058*, 379−385.
23. Deisenhofer, J., Epp, O., Miki, K., Huber, R., and Michel, H. (1985) *Nature 318*, 618−624.
24. Rigby, S. E. J., Nugent, J. H. A., and O'Malley, P. J. (1994) *Biochemistry 33*, 10043−10050.
25. Noguchi, T., Tomo, T., and Inoue, Y. (1998) *Biochemistry 37*, 13614−13625.
26. Ballschmiter, K., and Katz, J. J. (1969) *J. Am. Chem. Soc. 91*, 2661−2677.
27. Bekárek, V., Kaplanová, M., and Socha, J. (1979) *Stud. Biophys. 77*, 21−24.
28. Koyama, Y., Umemoto, Y., and Akamatsu, A. (1986) *J. Mol. Struct. 146*, 273−287.
29. Krawczyk, S. (1989) *Biochim. Biophys. Acta 976*, 140−149.
30. Noguchi, T., Inoue, Y., and Satoh, K. (1993) *Biochemistry 32*, 7186−7195.
31. Breton, J., Hienerwadel, R., and Nabedryk, E. (1997) in *Spectroscopy of Biological Molecules: Modern Trends* (Carmona, P., Navarro, R., and Hernanz, A., Eds.) pp 101−102, Kluwer, Dordrecht, The Netherlands.
32. Tomo, T., and Satoh, K. (1994) *FEBS Lett. 351*, 27−30.
33. Yuzawa, T., Kato, C., George, M. W., and Hamaguchi, H. (1994) *Appl. Spectrosc. 48*, 684−690.
34. Nabedryk, E., Andrianambinintsoa, S., Berger, G., Leonhard, M., Mäntele, W., and Breton, J. (1990) *Biochim. Biophys. Acta 1016*, 49−54.
35. Hofrichter, J., Henry, E. R., Sommer, J. H., Deutsch, R., Ikeda-Saito, M., Yonetani, T., and Eaton, W. A. (1985) *Biochemistry 24*, 2667−2679.
36. Hug, S. J., Lewis, J. W., Einterz, C. M., Thorgeirsson, T. E., and Kliger, D. S. (1990) *Biochemistry 29*, 1475−1485.
37. Sasaki, J., Yuzawa, T., Kandori, H., Maeda, A., and Hamaguchi, H. (1995) *Biophys. J. 68*, 2073−2080.
38. Nabedryk, E., Leonhard, M., Mäntele, W., and Breton, J. (1990) *Biochemistry 29*, 3242−3247.
39. Schenck, C. C., Mathis, P., and Lutz, M. (1984) *Photochem. Photobiol. 39*, 407−417.
40. Frank, H. A., Chynwat, V., Posteraro, A., Hartwich, G., and Simonin, I., Scheer, H. (1996) *Photochem. Photobiol. 64*, 823−831.
41. Takiff, L., and Boxer, S. G. (1988) *J. Am. Chem. Soc. 110*, 4425−4426.
42. DeWinter, A., and Boxer, S. G. (1999) *J. Phys. Chem. B 103*, 8786−8789.
43. Dexter, D. L. (1952) *J. Chem. Phys. 21*, 836−850.
44. Cogdell, R. J., Monger, T. G., and Parson, W. W. (1975) *Biochim. Biophys. Acta 408*, 189−199.
45. Kamlowski, A., Frankemöller, L., van der Est, A., Stehlik, D., and Holzwarth, A. R. (1996) *Ber. Bunsen-Ges. 100*, 2045−2051.
46. Bosch, M. K., Proskuryakov, I. I., Gast, P., and Hoff, A. J. (1996) *J. Phys. Chem. 100*, 2384−2390.
47. Stewart, D. H., Cua, A., Chisholm, D. A., Diner, B. A., Bocian, D. F., and Brudvig, G. W. (1998) *Biochemistry 37*, 10040−10046.
48. Koulougliotis, D., Innes, J. B., and Brudvig, G. W. (1994) *Biochemistry 33*, 11814−11822.
49. Nugent, J. H. A. (1996) *Eur. J. Biochem. 237*, 519−531.
50. Xiong, J., Subramaniam, S., and Govindjee (1998) *Photosynth. Res. 56*, 229−254.
51. Noguchi, T., and Inoue, Y. (1995) *FEBS Lett. 370*, 241−244.
52. Van Mieghem, F., Brettle, K., Hillmann, B., Kamlowski, A., Rutherford, A. W., and Schlodder, E. (1995) *Biochemistry 34*, 4798−4813.
53. Christensen, R. L. (1999) in *The Photochemistry of Carotenoids* (Frank, H. A., Young, A. J., Britton, G., and Cogdell, R. J., Eds.) pp 137−159, Kluwer, Dordrecht, The Netherlands.
54. Peterman, E. J. G., Dukker, F. M., van Grondelle, R., and van Amerongen, H. (1995) *Biophys. J. 69*, 2670−2678.

55. Carbonera, D., Giacometti, G., Agostini, G., Angerhofer, A., and Aust, V. (1992) *Chem. Phys. Lett. 194*, 275−281.
56. Kleima, F. J., Wendling, M., Hofmann, E., Peterman, E. J. G., van Grondelle, R., and van Amerongen, H. (2000) *Biochemistry 39*, 5184−5195.
57. Van Dorssen, R. J., Breton, J., Plijter, J. J., Satoh, K., van Gorkom, H. J., and Amesz, J. (1987) *Biochim. Biophys. Acta 893*, 267−274.
58. Kwa, S. L. S., Newell, W. R., van Grondelle, R., and Dekker, J. P. (1992) *Biochim. Biophys. Acta 1099*, 193−202.
59. Tomo, T., Mimuro, M., Iwaki, M., Kobayashi, K., Itoh, S., and Satoh, K. (1997) *Biochim. Biophys. Acta 1321*, 21−30.
60. Shuvalov, V. A., and Parson, W. W. (1981) *Biochim. Biophys. Acta 638*, 50−59.
61. Deligiannakis, Y., and Rutherford, A. W. (1998) *Biochim. Biophys. Acta 1365*, 354−362.
62. Durrant, J. R., Klug, D. R., Kwa, S. L. S., van Grondelle, R., Porter, G., and Dekker, J. P. (1995) *Proc. Natl. Acad. Sci. U.S.A. 92*, 4798−4802.

BI0019848